Compensation Mechanisms and Functionality of Transition Metal Oxide Surfaces and Interfaces: A Density Functional Theory Study

Rossitza Pentcheva, Narasimham Mulakaluri, Wolfgang Moritz, Warren E. Pickett, Hans-Georg Kleinhenz and Matthias Scheffler

Abstract The valence discontinuity at transition metal oxide surfaces and interfaces can lead to properties and functionality that are not observed in the respective bulk phases. In this contribution we give insight from density functional theory calculations on the emergence of conductivity and magnetism at the interfaces between (nonmagnetic or antiferromagnetic) insulators like $LaTiO_3$ and $SrTiO_3$ as well as $LaAlO_3$ and $SrTiO_3$, and investigate systematically the influence of water adsorption on the surface properties of Fe_3O_4. Additionally we present benchmarks for the performance of the full-potential linearized augmented plane wave method as implemented in the WIEN2k-code on HLRBI and HLRBII.

1 Introduction

The surfaces and interfaces of transition metal oxides represent a natural disruption of the bulk charge neutrality and a multitude of unexpected properties have been observed that differ substantially from the ones of the corresponding bulk materials. In order to understand naturally occurring phenomena as well as to selectively manipulate materials' properties like conductivity, magnetism and reactivity for technological applications, it is essential to gain a microscopic knowledge of the mechanisms

R. Pentcheva · N. Mulakaluri · W. Moritz
Department of Earth and Environmental Sciences, Section Crystallography, University of Munich, Theresienstr. 41, 80333 Munich, Germany
e-mail: rossitza.pentcheva@lrz.uni-muenchen.de

W.E. Pickett
Department of Physics, University of California at Davis, ???, USA
e-mail: pickett@physics.ucdavis.edu

H.-G. Kleinhenz
Leibniz-Rechenzentrum, Boltzmannstr. 1, 85748 Garching, Germany
e-mail: hgk@lrz.de

M. Scheffler
Fritz-Haber-Institut der Max-Planck-Gesellschaft, Faradayweg 4-6, 14195 Berlin, Germany
e-mail: scheffler@fhi-berlin.mpg.de

of charge accommodation and the resulting structural and electronic relaxations at oxide surfaces and interfaces.

In the first part of the project, we have systematically investigated the surface termination of $Fe_3O_4(001)$ and have found that a hitherto ignored bulk termination containing oxygen and octahedral iron is stabilized [1, 2]. A Jahn-Teller distortion was identified as the origin of the observed $(\sqrt{2} \times \sqrt{2})R45°$-reconstruction. Experimental evidence is given by scanning tunneling microscopy [3] as well as x-ray and low electron energy diffraction (XRD and LEED) measurements and quantitative analysis [1, 4]. The interaction of water with a mineral surface can be used as a probe of the surface reactivity and is a fundamental process both in nature and technology. In Sect. 4.1 we are studying how the adsorption of water influences the surface reconstruction, stability and properties of $Fe_3O_4(001)$.

Recently, the conductivity measured at the interfaces between the Mott insulator $LaTiO_3$ (LTO) and the band insulator $SrTiO_3$ (STO) but also between the two simple band insulators $LaAlO_3$ (LAO) and STO [5, 6] has fueled intensive research both on the theoretical and experimental side. In Sect. 4.2 we show how the charge mismatch at these interfaces together with electronic correlations can lead to the stabilization of novel charge, orbital and magnetically ordered phases [7, 8].

Prior to presenting the scientific results, we briefly describe the method in Sect. 2 and discuss the performance of WIEN2k-code on HLRBI and HLRBII in Sect. 3.

2 Method

Density functional theory (DFT) is a powerful tool to study the physical properties of crystals and surfaces. However, the high accuracy goes hand in hand with a high numerical demand, thus restricting DFT calculations to system sizes of the order of 10^2 atoms and 1000 electrons. Transition metal oxide surfaces and interfaces represent a particularly challenging task due to their complex structure, strong relaxations and surface reconstructions, the treatment of $3d$ electrons, the localized orbitals of oxygen and magnetism. The method we have chosen is the full-potential augmented plane waves (FP-LAPW) method in the WIEN2k-implementation [9]. As an all-electron method with atom-centered basis functions around the nuclei with a well defined angular momentum and plane waves in the interstitial region it is particularly suitable for the questions of interest. In order to investigate charge ordering phenomena at oxide surfaces and interface and to explore the role of electronic correlations, the LDA+U method in the fully localized limit [10] is used.

As generally known, DFT is a ($p = 0$ Pa, $T = 0$ K) method. Combining DFT with thermodynamics allows us to extend the predictive power of DFT to finite temperatures and pressures in the atmosphere. In the previous project period we have applied the *ab initio* thermodynamics formalism [11, 12] to investigate the influence of the oxygen pressure and temperature on the surface termination of $Fe_3O_4(001)$. In the current project we extend the phase diagram to account for the presence of hydrogen and water in the atmosphere. The lowest energy configuration of a surface in thermodynamic equilibrium with a humid environment with partial pressure p_{O_2},

p_{H_2O} and temperature T minimizes the surface energy, $\gamma(T, p)$, which depends on the Gibbs free energy of the surface and the chemical potentials of the constituents:

$$\gamma(T, p) = \frac{1}{2A}[G^{slab}_{Fe_3O_4(001)} - N_{Fe}\mu_{Fe}(T, p) - N_O\mu_O(T, p) - N_{H_2O}\mu_{H_2O}(T, p)]. \quad (1)$$

Applying the line of argument stated in Ref. [12] we can substitute the terms in (1) by quantities accessible to DFT-calculations. As mentioned above to solve the all-electron Kohn-Sham equations we use the full-potential augmented plane waves (FP-LAPW) method in the WIEN2k-implementation [9] and the generalized gradient approximation (GGA) in the parameterization of Perdew, Burke and Ernzernhof [13].

3 Performance of WIEN2k on HLRBI and HLRBII

The fine grain parallel version of the WIEN2k-code was ported to and optimized for the Hitachi-SR8000 in collaboration with the Leibniz Rechenzentrum (LRZ). A detailed report of the optimization steps and the extensive benchmarks on SR8000 and IBM Regatta (RZ Garching) is given in Ref. [2].

The migration to the HLRBII SGI-Altix 4700 was completed in the last two years again in close collaboration with the LRZ. Currently both the fine grain parallel version (MPI) and the k-point parallelization scheme are used in the production. A hardware description of the HLRBI and HLRBII is given in Table 1. Here, we have done detailed benchmarks of the performance on HLRBII (second stage) and have compared these to previous ones on the HLRBI.

We have used two systems for the benchmarks: A 0.5 ML A-termination of $Fe_3O_4(001)$ containing 70 atoms in the unit cell to compare with previous benchmarks on HLRBI. Here the cutoff for the plane wave basis set was set to $E_{cut} = 19$ Ry which corresponds to a matrix size of 15000. The second benchmark case is a typical system used currently to study the water adsorption on $Fe_3O_4(001)$. With its 130 atoms and 1050 electrons per unit cell, it corresponds to the biggest systems currently under consideration. The adsorption of water on the $Fe_3O_4(001)$-surface represents a computational challenge—due to the short O-H-bond the muffin tin

Table 1 Hardware Description of HLRBI (Hitachi's SR8000) and HLRBII (SGI Altix 4700—second stage) and performance of `lapw1`

	Hitachi SR8000	SGI Altix 4700
Clock rate	0.375 GHZ	1.6 GHZ
Peak/core	1.5 GFlop/s	6.4 GFlop/s
Memory BW/core	0.5 GBytes/s	2.12 GBytes/s
Performance of `diag` per core (8 cores)	0.450 GFlops/s	1.87 GFlop/s
Percent of peak performance	30	28(38-BW)

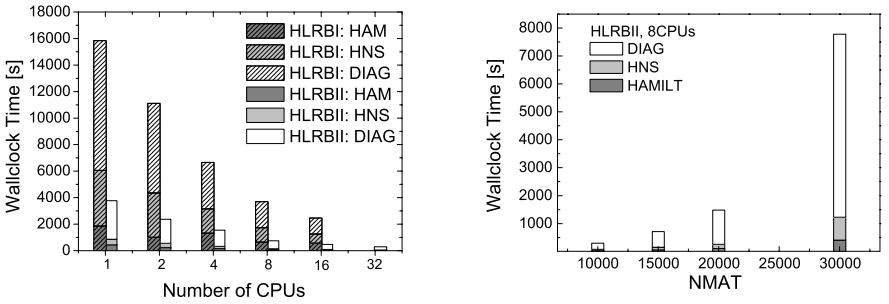

Fig. 1 *Left panel*: Comparison of running times for the different parts of `lapw1` (`hamilt`, `hns` and `diag`) for $N_{mat} = 15000$ as a function of N_{CPU} on Hitachi SR-8000 and SGI Altix 4700. *Right panel*: Running times of `lapw1` for different matrix sizes on 8 cores on HLRBII

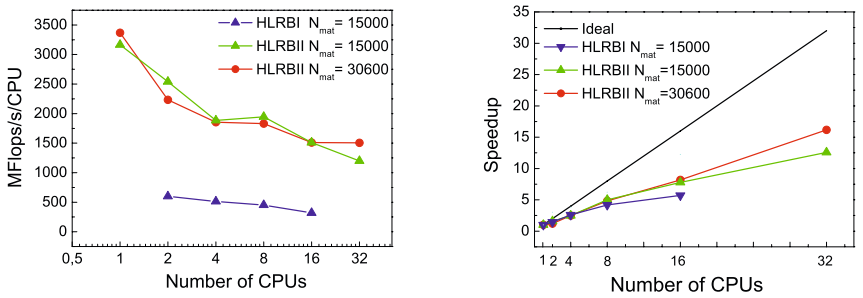

Fig. 2 *Left panel*: Performance of `lapw1` per core as a function of N_{CPU}. *Right panel*: Speedup on HLRBI ($N_{mat} = 15000$) and HLRBII ($N_{mat} = 15000$ and 30600)

radii of oxygen (and hydrogen) have to be substantially reduced. The consequence is that a much higher cutoff parameter for the wave functions and potential is needed in order to achieve the same accuracy as for the clean $Fe_3O_4(001)$-surface. This leads to a matrix dimension of $N_{mat} = 30600$.

The results of the benchmarks are displayed in Figs. 1, 2 and Table 1. The most time-consuming step in WIEN2k is `lapw1` where approximately 80–90% of the computational time is spent. As can be seen from Fig. 1 (right panel), the latter scales exponentially with the size of the matrix. Generally, the computational time in `lapw1` is reduced by a factor of 4–5 on HLRBII compared to HLRBI. To a large extent this can be attributed to the change of core clock rate (375 MHz vs 1600 MHz). `lapw1` contains the set up of the Hamiltonian (subroutine `hamilt`), its non-spherical part (subroutine `hns`) and the diagonalization (subroutine `diag`). Reprogramming of the MPI parallelization in the last version (07.03) of WIEN2k led to a substantial reduction of the computational time of `hns` from up to 30% on HLRBI to approx. 10% in the current version on HLRBII. On Hitachi SR-8000 `lapw1` showed an acceptable scaling up to 8 CPUs (one node) which however breaks down when using more than one node (cf. Fig. 2). The scaling behavior of

the fine grain parallel version on HLRBII is much better and preserves a nearly linear behavior beyond 8 CPUs, especially for large system sizes of $N_{mat} = 30600$.

As can be seen from Table 1 the peak performance per core of HLRBII is four times higher than Hitachi's SR8000. We find that the effective performance of `diag` is about 30% of the peak performance on both HLRBI and II, which is an excellent value for this type of code. We have experienced that the memory bandwidth has influence on the performance of the major routines of `lapw1`. Partitions with low density blades (2 cores per memory path) show a further performance improvement of 25% compared to the high density blades (4 cores per memory path) given in Table 1. The performance on the low density blades is 2.4 Gflop/s per core or 38% of peak performance.

4 Scientific Results

4.1 Adsorption of Water on $Fe_3O_4(001)$

The interaction of water with a mineral surface is a fundamental process both in nature and technology (e.g. catalysis) and a first step in understanding surface reactivity. Magnetite plays an important role in the adsorption and reduction of heavy metal ions (Cr, As) and other contaminants [14, 15]. These processes typically take place in aqueous solutions. Therefore, it is important to understand how water adsorption influences the stability and properties of the $Fe_3O_4(001)$-surface.

Magnetite crystallizes in the inverse spinel structure, where in [001]-direction B-layers, containing oxygen and octahedral iron, alternate with A-layers with tetrahedral iron. Starting from the modified B-layer, found to be most stable on the clean surface [1] and shown in Fig. 3(a) as well as an A-layer termination where every second tetrahedral iron is missing (0.5 A-layer), we have varied the degree of hydroxylation of the surface. These calculations are computationally very involved, because due to the short OH-bond length the muffin tin of hydrogen is very small ($R_{mt}^{\mathrm{H}} = 0.6$ a.u., $R_{mt}^{\mathrm{O}} = 1.1$ a.u.), and this requires a very high plane wave cutoff to obtain good convergence (currently $E^{wf} = 25$ Ry). Because surface relaxations involve deeper layers and to avoid spurious interaction between the surface layers we are using a slab containing seven B-layers and 10–12 Å of vacuum to separate the surfaces in z-direction. On the average, the considered systems contain 130 atoms and 1050 electrons which results in matrix sizes of 30600. On 8 CPUs the computational time for the setup and diagonalization of the Hamiltonian matrix (`lapw1`) is 6553 s/core (on 8 cores). In spin-polarized calculations `lapw1` is performed for both spin directions separately and we use 4 k_{II}-points for the integration in the irreducible part of the Brillouin zone (IBZ). The full geometry optimization of each system requires on the average 10 geometry steps and for each geometry step approximately 20–40 iterations are needed to reach convergence of the energy and electron density.

One aspect that we want to resolve is the mode of adsorption of water: molecular versus dissociative. Therefore we are also studying different adsorption mechanisms

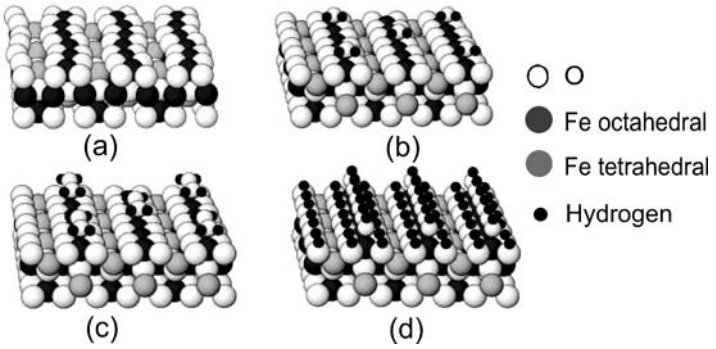

Fig. 3 Models of the $Fe_3O_4(001)$-surface (**a**) clean surface showing the Jahn-Teller distorted B-layer termination; (**b**) and (**c**) B-layer termination covered by one or two H_2O molecules per unit cell; (**d**) a fully hydroxylated B-layer termination

of a single water molecule as well as two H_2O molecules in the surface unit cell. Some adsorbate geometries are shown in Fig. 3(b) and (c). Preliminary results indicate that molecular adsorption (Fig. 3(b)) is more favorable for low coverages but already for two water molecules per surface cell the two mechanisms have close energies. To compare the stability of the different configurations, the surface phase diagram of the clean $Fe_3O_4(001)$-surface [1] is extended to account for both the O_2 and H_2O partial pressure. We find that a completely hydroxylated B-layer with OH-groups on top of octahedral iron and all surface oxygen being substituted by OH-groups, shown in Fig. 3(d), is the most stable configuration at water rich conditions. The results of the structural optimization reveal that the adsorption of water tends to suppress and even lift up the $(\sqrt{2} \times \sqrt{2})R45°$-reconstruction observed on the clean surface. Preliminary LEED measurements performed in parallel to the calculations support this interesting prediction. The geometries obtained from DFT are currently used as a starting point for a quantitative LEED-analysis as already done for the clean surface [4].

4.2 Charge Accommodation at Digital Perovskite Superlattices

The fabrication of perovskite superlattices with an atomic control of the number of layers of each material was recently demonstrated using pulsed laser deposition [5]. This achievement of today's growth techniques has invigorated intensive research. The reason is that the interfaces, that are generated, show novel properties that do not exist in the parent compounds. Examples are the two-dimensional electron gas (2DEG) measured at the interfaces between the Mott insulator $LaTiO_3$ (LTO) and the band insulator $SrTiO_3$ (STO) [5], but also between the two simple band insulators $LaAlO_3$ (LAO) and STO [6]. Perovskites possess a natural charge modulation in the [001]-direction, e.g. in LTO positively charged $(LaO)^+$ layers alternate with negatively charged $(TiO_2)^-$, while in STO both the SrO and TiO_2-layers are

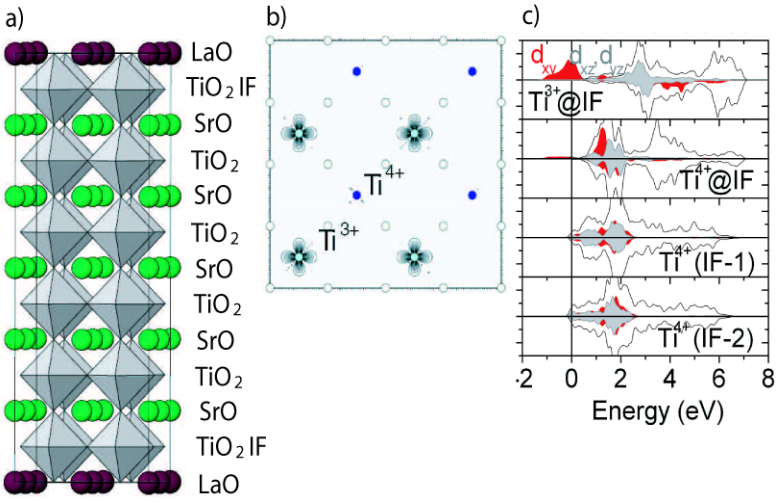

Fig. 4 (**a**) Side view of a $(LTO)_1/STO_5$ superlattice; (**b**) charge distribution of the 3*d* states in the interface TiO_2-layer, showing a charge and orbitally ordered checkerboard arrangement of Ti^{3+} and Ti^{4+}; (**c**) layer resolved density of states showing the Ti 3*d* states across the interface for a relaxed $(LTO)_1/STO_5$ superlattice (from Ref. [8])

neutral. Thus the interface (IF) between these two insulators represents a simple realization of a polar discontinuity and poses the question of how charge mismatch is accommodated and whether insulating behavior can be preserved. In the other system, LAO/STO, both the A and B sublattice cations in the perovskite structure change across the interface giving rise to two different types of interfaces: an *n*-type between a LaO and a TiO_2-layer, that was found conducting with a high electron mobility and a *p*-type between a SrO and an AlO_2-layer that showed insulating behavior despite the charge mismatch [6].

In order to investigate the compensation mechanism using the material specific insight from first principles and in particular to explore the role of electronic correlations, we have performed DFT calculations including a Coulomb repulsion U [10] for a variety of LTO_n/STO_m and LAO_n/STO_m superlattices. Here, we have varied the number of layers (n, m) of each material. These systems contain so far up to 100 atoms and 800 electrons ($N_{mat} = 14500$). The computational time of `lapw1` per CPU (on 8 CPUs) per *k*-point is 2800 s. We note that all cases are spin-polarized and that at least 6 k_{II}-points are used in the IBZ.

Figure 4(a) shows a side view of a LTO_1/STO_5. Our LDA+U calculations [8] predict that the charge mismatch at this interface is accommodated by a charge disproportionation: A charge and orbitally ordered IF-layer is found with Ti^{3+} and Ti^{4+} ordered in a checkerboard manner (see Fig. 4(b)). At the Ti^{3+}-sites the d_{xy}-orbital is occupied. While the system is insulating for the structure with bulk positions of the atoms, lattice relaxations lead to the experimentally observed conducting behavior. A similar compensation mechanism is found also for the *n*-type interface of LAO and STO [7]. Although both LAO and STO are nonmagnetic and LTO is

an antiferromagnet of G-type, a new magnetic phase emerges at the IF with diluted Ti^{3+}-spins that have a slight preference to antiferromagnetic coupling (with a larger periodicity than LTO bulk) [7, 8]. Brinkman et al. recently found first experimental indications for localized magnetic moments at the *n*-type LAO/STO IF [16] supporting our prediction. Since these superlattices are strained due to the lattice mismatch between the bulk compounds, we are currently investigating the effect of interlayer relaxations on the properties of the interface.

At the *p*-type LAO/STO interface (AlO_2-layer next to a SrO-layer at the interface) we have investigated two compensation mechanisms: (i) at a structurally ideal interface, as suggested by the initial results of Ohtomo and Hwang [6], insulating behavior can only be obtained by a charge disproportionation on the oxygen sublattice with a charge and magnetically ordered OP_π hole localized at a quarter of the oxygens in the AlO_2-layer [7]; (ii) oxygen vacancies, suggested in several more recent experimental studies (e.g. [17]), are a natural way to compensate the excess hole at the interface. We have studied vacancies in the AlO_2- and SrO-layer and find that in both cases the Fermi level lies in a dip of the density of states.

These results show that in materials with multivalent ions charge disproportionation offers an additional, correlation driven compensation mechanism, unanticipated e.g. in polar semiconductor interfaces.

Acknowledgements We acknowledge support by the German Science Foundation, European Science Foundation within EUROMINSCI and the Bavaria California Center of Technology (BaCaTec). N.M. acknowledges a fellowship by the Max-Planck Society.

References

1. R. Pentcheva, F. Wendler, H.L. Meyerheim, W. Moritz, N. Jedrecy, M. Scheffler, Phys. Rev. Lett. **94**, 126101 (2005)
2. R. Pentcheva, F. Wagner, W. Moritz, M. Scheffler, Structure, energetics and properties of Fe_3O_4(001) from first principles, in *High Performance Computing in Science and Engineering*, Munich, 2004 (Springer, Heidelberg, 2005), pp. 375–381
3. M. Fonin, R. Pentcheva, Yu.S. Dedkov, M. Sperrlich, D.V. Vyalikh, M. Scheffler, U. Rüdiger, G. Güntherodt, Phys. Rev. B **72**, 104436 (2005)
4. R. Pentcheva, W. Moritz, J. Rundgren, S. Frank, D. Schrupp, M. Scheffler, A combined DFT/LEED-approach for complex oxide surface structure determination: Fe_3O_4(001). Surf. Sci. (2008). doi:10.1016/j.susc.2008.01.006
5. A. Ohtomo, D.A. Muller, J.L. Grazul, H.Y. Hwang, Nature **419**, 378 (2002)
6. A. Ohtomo, H.Y. Hwang, Nature **427**, 423 (2004)
7. R. Pentcheva, W.E. Pickett, Phys. Rev. B **74**, 035112 (2006)
8. R. Pentcheva, W.E. Pickett, Phys. Rev. Lett. **99**, 016802 (2007)
9. P. Blaha, K. Schwarz, G.K.H. Madsen, D. Kvasnicka, J. Luitz, *WIEN2k, an Augmented Plane Wave + Local Orbitals Program for Calculating Crystal Properties* (Karlheinz Schwarz, Techn. Univ. Wien, Wien, 2001). ISBN 3-9501031-1-2
10. V.I. Anisimov, I.V. Solovyev, M.A. Korotin, M.T. Czyzyk, G.A. Sawatzky, Phys. Rev. B **48**, 16929 (1993)
11. C.M. Weinert, M. Scheffler, in *Defects in Semiconductors*, ed. by H.J. Bardeleben. Mat. Sci. Forum, vols. 10–12 (1986), p. 25
12. K. Reuter, M. Scheffler, Phys. Rev. B **65**, 035406 (2002)

13. J.P. Perdew, K. Burke, M. Ernzerhof, Phys. Rev. Lett. **77**, 3865 (1996)
14. K. Ohe, Y. Tagai, S. Nakamura, T. Oshima, Y. Baba, J. Chem. Eng. Jpn. **38**(8), 671 (2005)
15. H. Katsumata, S. Kaneco, K. Inomata, K. Itoh, K. Funasaka, K. Masuyama, T. Suzuki, K. Ohta, J. Environ. Manag. **69**, 187 (2003)
16. A. Brinkman, M. Huijben, M. van Zalk, J. Huijben, U. Zeitler, J.C. Maan, W.G. van der Wiel, G. Rijnders, D.H.A. Blank, H. Hilgenkamp, Nature Mater. **6**, 493 (2007)
17. N. Nakagawa, H.Y. Hwang, D.A. Muller, Nature Mater. **5**, 204 (2006)